Journal of Applied Geophysics 134 (2016) 36–43

Contents lists available at ScienceDirect

Journal of Applied Geophysics

journal homepage: www.elsevier.com/locate/jappgeo

A novel reconstruction method based on changes in phase for subsurface large sloped dielectric target using GPR

Lijun Zhou [a], Shan Ouyang [b,*], Guisheng Liao [a]

[a] School of Electronic Engineering, Xidian University, Xi'an 710071, People's Republic of China
[b] School of Information and Communications, Guilin University of Electronic Technology, Guilin 541004, People's Republic of China

ARTICLE INFO

Article history:
Received 13 August 2015
Received in revised form 1 August 2016
Accepted 23 August 2016
Available online 26 August 2016

Keywords:
Geometric features
Reconstruction
Phase
Dielectric target
Virtual image

ABSTRACT

In ground-penetrating radar (GPR) subsurface target reconstruction, various techniques based on amplitude (or energy) information of echoes from metal target with small size can work well. However, for environmental and geological applications, the quantitative analysis of the target's geometric features, like location, shape and size, is exactly what we are concerned about. Amplitude-based reconstruction method faces challenges in these applications. A large sloped target under the surface may lead to abundant virtual image energy and cause position deviation. In addition, the echoes from the inner part of the penetrable dielectric target may be too weak to be detected. However, changes in phase may highlight the effects of echoes from the target on that from the surroundings, even if the effect is small due to the weak energy. In this paper, a novel method based on changes in phase is proposed to reconstruct subsurface large sloped dielectric target. To remove the virtual image, the main idea is based on the geometric relationship between the recorded signal plotted beneath the receiving antenna and the reflected signal emanated from the target position which is "ahead" or "behind" of the receiving antenna. Furthermore, the electromagnetic (EM) wave propagating through the penetrable target will change its velocity and result in advancing or lagging related to the geometric shape of the target. In this case, the weak echoes from the back surface of the target can be compensated according to the advancing or lagging. With the proposed method, the virtual image is eliminated and both front and back surface of the target are reconstructed. Results from the laboratory experiments demonstrate the validity of the proposed method.

1. Introduction

Reconstruction of the geometric features (i.e., location, shape, and size) of buried targets from ground-penetrating radar (GPR) data is of huge interest in environmental, geological, and other engineering applications (Catapano et al., 2008; Daniels, 2004). This kind of studies is particularly important for the noninvasive diagnoses of the subsurface fragments caused by roadbed settlement and non-layered pavement (Walton et al., 2015). In practice, the fractured roadbeds or paved layers are easily to sink to form a slope at a certain orientation. Usually, the fractured blocks are large in size with considerable thickness. Therefore, challenges may arise when the size, shape, and orientation of such geological anomalies are important.

Several approaches have been employed to reconstruct the geometric features of buried targets. Catapano et al. (2007, 2008) applied the sampling method (SM) to reconstruct the shape and location of buried targets. The SM and its improved methods possess the capability of providing accurate shape reconstruction and negligible computation burden. However, the improvement of the reconstructing accuracy is at the expense of the complex measurement stage, such as multipolarization multiview probes or multifrequency strategy. In addition, the overestimation of the target size would produce deformation of the target shape (Catapano et al., 2007). Valerio et al. (2011) applied an energy-based reconstruction approach for strong scattering targets. Due to the amplitude attenuation, the scattering echoes from the non-irradiated surface of the target were too weak to be detected to obtain a complete shape of the target. Nomura et al. (2011) applied the non-parameter estimation approach to attempt to reconstruct buried targets. In the research, the unknown parameters, such as the length, inclination angles and horizontal positions, were estimated for a buried flat-plate. However, the problem of ambiguous boundaries of hyperbolas from the target has not been solved and the shape estimation has not been considered yet.

The previous examples are mainly based on amplitude information of scattering echoes. As addressed above, the amplitude may suffer significant attenuation in propagation, while phase can remain unaltered for the usual travel time ranges (Neto and Medeiros, 2006; Sugak and Sugak, 2010). In fact, the phase of GPR signal may provide more information on subsurface properties (Huuskonen et al., 2015). For example, the reflecting boundary position, absorptive and dispersive features of media are embedded in the signal phase (Sugak and Sugak, 2010;

* Corresponding author.
E-mail address: hmoysh@guet.edu.cn (S. Ouyang).

http://dx.doi.org/10.1016/j.jappgeo.2016.08.013

Soldovieri et al., 2005). Recent years, phase has been applied in image reconstruction (Huuskonen et al., 2015; Mikhnev et al., 2012; Ni and Huo, 2007). Ni and Huo (2007) investigated the importance of phase information in signal/image reconstructions. Mikhnev et al. (2012) proposed a novel signal processing method based on the phase information to reconstruct the target location. Developed by this idea, Huuskonen et al. (2015) retrieved multiple buried targets with different permittivities by applying phase profiling method. Moreover, an important contribution of phase profile related to the GPR problem is to characterize the buried target via the phase change of the reflected waves from the target and surrounding medium. The phase change value around zero degrees probably indicates that there is no target in the background, and the larger phase change value may indicate a target with high permittivity compared to surrounding medium (Taner, 2001; Mikhnev et al., 2012; Huuskonen et al., 2015). It is worth to be noted that the weak echoes from non-metallic target can be also detected by means of phase information.

In this study, the sloped large target will lead to a great deal of virtual image with strong energy. The virtual image is closely related to the geometric feature of the target, such as the shape and the orientation. Thus, the true target profile will be surrounded by the virtual image. For this case, the reconstructed results based on energy detection will deviate from the true value. Furthermore, considering most fractured roadbeds or pavements is dielectric and penetrable, the electromagnetic wave (EM) propagating through the target will be attenuated in energy (Hipple von, 1995) and this part of weak energy is difficult to be detected by the energy detection. The purpose of this research is to reconstruct such large sloped dielectric target. A novel reconstruction method based on changes in phase of the GPR echoes is proposed to remove the virtual image and compensate the weak energy. In the proposed method, the GPR echo features and problems of subsurface large sloped dielectric target are analyzed. To solve these problems, corresponding algorithms based on changes in phase are presented.

2. GPR echo features of subsurface large sloped target

Fig. 1 shows the echo data acquisition model of a subsurface sloped target. Two layers are considered, as labeled as Layer 1 and Layer 2 in Fig. 1, respectively. The target is sloped located in Layer 1. The aim here is to detect such sloped target and reconstruct it. The GPR system samples the reflected echo at the GPR location to form an A-scan. A series of A-scans are arranged sequentially to form a B-scan when the GPR system moves along one test line in +X axis. At the other direction (Y axis), B-scans are obtained to form a C-scan when the GPR system moves along other test lines. Assume that the target is positive sloped when the GPR system is moving along +X axis. Relatively, if the GPR system is moving along −X axis, the target is negative sloped. Here we consider the positive case for an instance.

It is common known that the antennas of GPR radiate energy in patterns of lobes or beams and the main lobe can even be in the region of 90° (Skolnik, 2008). When the recorded signal is plotting beneath the receiving antenna, the reflected signal will emanate from the target position, which is “ahead” or “behind” of the receiving antenna. Therefore, a hyperbolic curve would be observed in the B-scan image from a target with circular cross section. The position of such target usually corresponds to the apex of this hyperbola. As a matter of fact, the position can be well determined for the target regarded as an ideal point scatterer. However, for a sloped large target, as shown in Fig. 1, the target can be regarded as the combination of multiple scattering centers. In this case, in the B-scan image, the hyperbolic curves from those scattering centers will be overlapped and the energy will be accumulated (Schofield et al., 2014). The upper scattering centers in range of radar

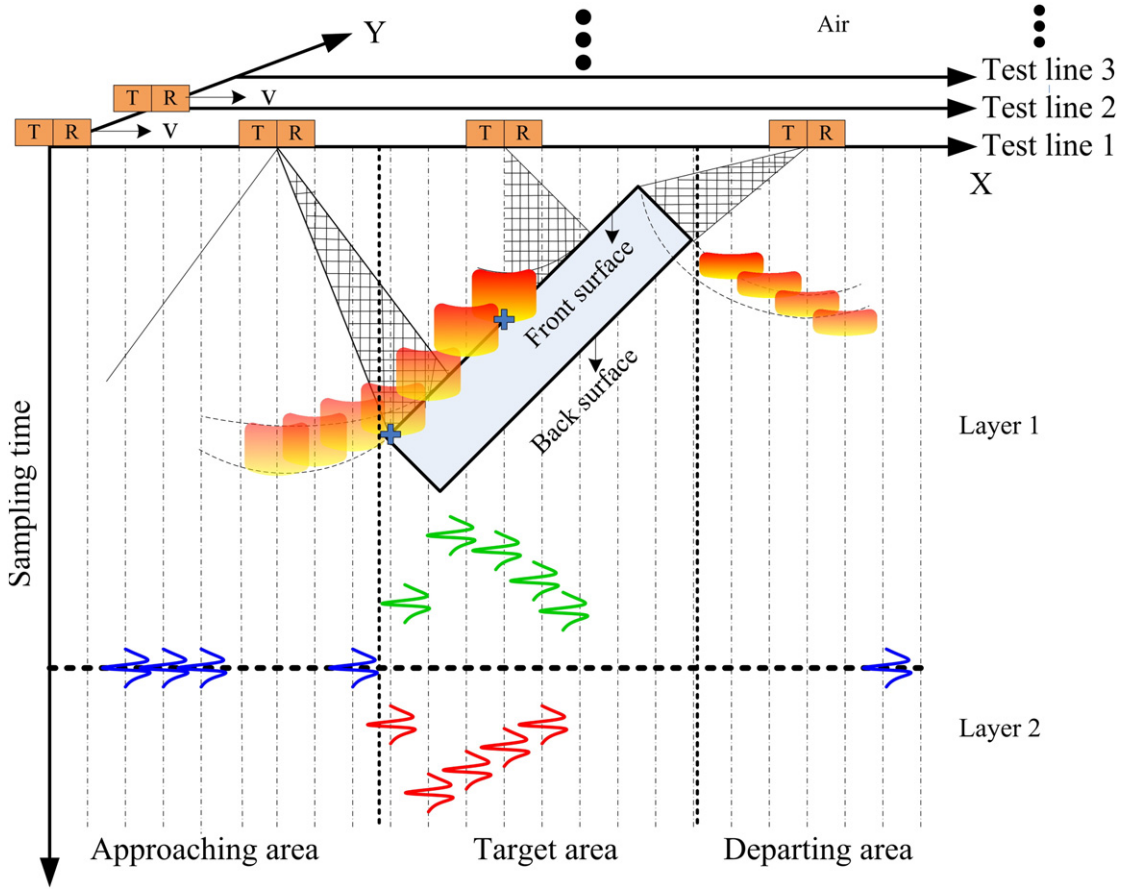

Fig. 1. Echo data acquisition model of subsurface sloped target.

lobes are close to the receiver and show stronger energy. It is obvious that the energy strength depends on the number of scattering centers in range of radar radiation, as well as the distance of scattering centers to the receiving antenna. Hence, when the GPR system is approaching to the target, more scattering centers of the target appearing in range of lobes of the antenna are illuminated by an incident wave, which results in the accumulated energy increasing (as shown in approaching area). When the GPR system is departing from the target, the scattering centers illuminated by the incident wave are reduced; then the accumulated energy is decreasing (as shown in departing area). For these cases, the echoes can also be received even if the GPR system is still outside the target area. Once the GPR system is moving across the target, the true position of the scattering center (the desired test point denoting with a cross) beneath the GPR system will be recorded by the A-scan. It should be noted that for the negative case, i.e., the GPR system moves along the −X axis, the proposed method is also valid. For this case, the scanning image remains the same and the difference is that the accumulated energy from the approaching area (denoted by departing area in Fig. 1 for the positive case) will be weaker than that from the departing area (denoted by approaching area in Fig. 1 for the positive case). This is because the number of scattering centers in range of radar radiation at the approaching area for negative case is much less than that for positive case. However, in either case, the energy from the upper part of the target (as shown in shadow, which can be regarded as undesired test points) will cover the energy from the desired test point due to the radar lobes. The energy from those undesired test points will result to interference for extraction of the true target position.

Consequently, during the measurement, the image of the true target is always enclosed by some image with strong energy from the echoes of those interfered scattering centers. In this paper, we call such interfered image as *virtual image*, which makes the target position deviate from the true position. Hence, the virtual image is necessary to be removed.

Furthermore, for a penetrable dielectric target, some part of the EM wave may reflect back to the receiver from the front surface of the target, and another part of the wave may penetrate the target and then reflect from its back surface. As stated in the previous section, some reflected echoes from back surface become weak, due to the geometric spreading. In order to reconstruct the whole target, the weak part echoes should be enhanced. In addition, it is well known that EM wave traveling in different media will change its velocity. This leads to two results: 1) if the dielectric constant of the target is larger than that of surroundings, the wave penetrating the target will delay arriving to the interface between Layer 1 and Layer 2 (as shown with red waves in Fig. 1) compared with the wave directly arrives to the interface without touching any obstacle (as shown with blue waves in Fig. 1), which is defined as *lagging* case; 2) if the dielectric constant of the target is less than that of surroundings, the wave penetrating the target arrives to the interface in advance (as shown with green waves in Fig. 1), which is defined as *advancing* case. In either case, the lagging or advancing indicates the geometric information of back surface of the target. With this respect, the profile of the back surface of the target can be determined by investigating the lagging or advancing case.

3. Proposed method

The reconstruction algorithm based on changes in phase is shown in Fig. 2. The data acquisition method remains the same as that shown in Fig. 1. The relative permittivities of Layer 1 and Layer 2 are given as ε_1 and ε_2, respectively. A positive sloped concrete with relative permittivity ε_3 is shown in Fig. 2. Here only a B-scan profile is given as an example to illustrate the proposed method due to the limitation of the space.

Step 1: For all A-scans received by the GPR moving along the test line, a B-scan $B(u,t)$ based on amplitude of the echoes is formed, as shown in Fig. 2(b). Here let $u=\Delta x\cdot n$ and $t=\Delta t\cdot m$, where Δx is the interval of test line and Δt is the sampling interval. For convenience, Δx and Δt are omitted and $B(u,t)$ can be written as $B(n,m)$, where $n=1,\ldots,N$, $m=1,\ldots,M$. It can be seen that the energy of echoes becomes weaker as the propagation depth increases. Considering interfaces between layers will be acquired for further analysis, the background should be calculated in this step. Here the former N_0 A-scans are extracted from original B-scan $B(n,m)$ to express the background information without target (Skolnik, 2008).

$$G(m)=\frac{1}{N_0}\sum_{n=1}^{N_0}B(n,m) \tag{1}$$

It should be noted that a proper original B-scan is needed to ensure that the target has not been located at the beginning of the surveying line. N_0 is usually given as $N/10$. In fact, $G(m)$ is the mean value of the former N_0 A-scans. Usually, the interfaces between layers will produce peaks in A-scans. In this case, the peaks of $G(m)$ are extracted to find interfaces. Assuming that there are Q layers, $Q+1$ interfaces can be extracted and denoted as $G(m_i)$, $i=0,1,\ldots,Q$. For a given example shown in Fig. 2, two peaks $G(m_0)$ and $G(m_1)$ are extracted, representing the interfaces between air and Layer 1, Layer 1 and Layer 2, respectively.

Step 2: Hilbert transform is carried out for Fig. 2(b) to yield phase profile $H(n,m)$ (Huuskonen et al., 2015) as shown in Fig. 2(c). The phase profile shows remarkable information of echoes even for the weak ones.

Step 3: In order to highlight the prominent characteristic about target, changes in phase are obtained by deriving the phase profile $H(n,m)$ with respect to distance, i.e.,

$$D(n,m)=\frac{dH(n,m)}{dn} \tag{2}$$

If there is no interference in background, D will remain zero, otherwise, D will be non-zero. Thus the positions of changes in phase are points where $D(n,m)\neq 0$, i.e.,

$$(\boldsymbol{X},\boldsymbol{Y})=\{(n,m)|D(n,m)\neq 0; m=1,\ldots,M, n=1,\ldots,N\} \tag{3}$$

where $\boldsymbol{X}=[x_1,\cdots,x_f]^T$ and $\boldsymbol{Y}=[y_1,\cdots,y_f]^T$ indicate the test line position and sampling time position of changes in phase, respectively, as shown with red area in Fig. 2(d). In Fig. 2, several points from $(\boldsymbol{X},\boldsymbol{Y})$ are specifically marked (such as '●', '▲', '□', and '★') to interpret the algorithm. It can be noted that the horizontal events (or the background) from the GPR profile can be removed by Step 3.

Step 4: In this step, the target points and virtual image points from the changes in phase will be discriminated. Along the moving trace of GPR system, the virtual image should appear firstly at the approaching area, then at the target area, and last at the departing area, as shown in Fig. 1.

The position of the receiving antenna is set as (a,b). At the position (a,b), the point of changes in phase existing in the recorded signal beneath the receiving antenna is denoted as (a,y). Assume that this point as virtual image point. Then an arbitrary point $(x_i,y_i)\in(\boldsymbol{X},\boldsymbol{Y})$ and $(x_i,y_i)\neq(a,y)$ satisfied the Eq. (4)

$$(x_i-a)^2+\left[(y_i-b)\frac{c}{\sqrt{\varepsilon_1}}\right]^2=\left[(y-b)\frac{c}{\sqrt{\varepsilon_1}}\right]^2 \tag{4}$$

is the corresponding true target point. Here Eq. (4) indicates the geometric relationship between the recorded signal beneath the receiving antenna and the reflected signal emanated from the target position which is "ahead" or "behind" of the receiving antenna. Then define the true target set $(\boldsymbol{R}^1,\boldsymbol{W}^1)=\{(x_{rw},y_{rw})\}$ with $(x_i,y_i)\in(\boldsymbol{R}^1,\boldsymbol{W}^1)$ and virtual image set $(\boldsymbol{K},\boldsymbol{S})=\{(x_{ks},y_{ks})\}$ with $(a,y)\in(\boldsymbol{K},\boldsymbol{S})$.

Until now, virtual image points and true target points have been discriminated, as shown in Fig. 2(e). Here c is the light speed. In this paper,

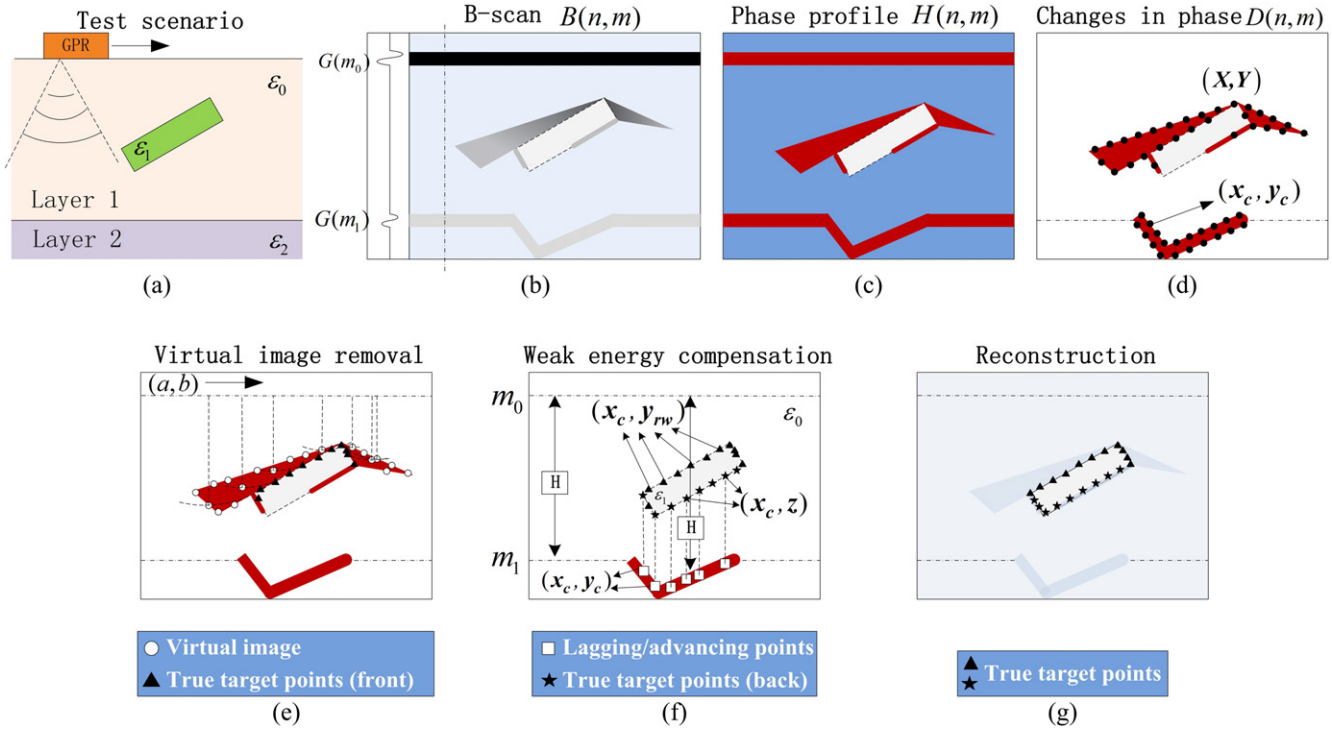

Fig. 2. Illustration of the procedure of the proposed method.

the permittivities of the concrete slab and survey environment are prior estimated using the method provided by Daniels (2004) and Hipple von (1995). Notably, in the 2D-coordinate throughout this paper, the former means the position of the along track of test line and the latter indicates the sampling time.

Step 5: As analyzed in the previous section, the lagging or advancing indicates the geometric information of back surface of the target. This feature is useful to compensate the weak energy from the back surface of the target. In order to extract the lagging or advancing automatically, firstly the interfaces between layers should be obtained. Since the phenomenon of lagging or advancing appears in interfaces, search the m_i interface in Eq. (1) using the nearest neighbor searching method (Liu and Wei, 2015) to find the lagging or advancing points (x_c,y_c) caused by target, as shown in Fig. 2(d). In the nearest neighbor searching method, the squared Euclidean distance between points of the m_i interface is calculated at directions of test line and depth. If the squared Euclidean distance is larger than a threshold, there exists lagging or advancing points on the m_i interface; on the contrary, there is no lagging or advancing point on the m_i interface. The threshold is given as the average distance value of points on the m_i interface. Here $(x_c,y_c)\in(\boldsymbol{X},\boldsymbol{Y})$, as shown in Fig. 2(d). In Fig. 2(f), it can be seen that the depth H of Layer 1 can be not only estimated by the surface position m_0 and the end position m_1 of Layer 1 without a target, i.e.,

$$H=\frac{c(m_1-m_0)}{2\sqrt{\varepsilon_1}} \tag{5a}$$

but also estimated by m_0 and the lagging or advancing position of Layer 1 with a target, i.e.,

$$H=\frac{1}{2}\left[(y_{rw}-m_0)\frac{c}{\sqrt{\varepsilon_1}}+(z-y_{rw})\frac{c}{\sqrt{\varepsilon_3}}+(y_c-z)\frac{c}{\sqrt{\varepsilon_1}}\right] \tag{5b}$$

where (x_c,y_c), (x_c,z) and (x_{rw},y_{rw}) are the positions of lagging or advancing point, back surface point of the target, and true target point, respectively. Here the true target point (x_{rw},y_{rw}) obtained from Step 4 is assumed as front surface point. The transform from sampling time to depth is based on the relationship $D=ct/2\sqrt{\varepsilon_1}$ (Chlaib et al., 2014). Subsequently, under the condition $\varepsilon_1\neq\varepsilon_3$, the time position z can be obtained according to Eqs. (5a) and (5b), i.e.,

$$z=\frac{(m_1-y_{rw}-y_c)\sqrt{\varepsilon_3}+y_{rw}\sqrt{\varepsilon_1}}{\sqrt{\varepsilon_1}-\sqrt{\varepsilon_3}} \tag{6}$$

It can be observed from Eq. (6) that z depends on the dielectric constants of surroundings and the target, the true target time position of the front surface, the interface between Layer 1 and Layer 2, and the lagging or advancing points. For the case of lagging, $\varepsilon_3>\varepsilon_1$, and then $y_c>m_1$. For the case of advancing, $\varepsilon_3<\varepsilon_1$, and then $y_c<m_1$. This coincides with the results stated in the previous section. In particular case $\varepsilon_3=\varepsilon_1$, according to Eqs. (5a) and (5b), then $y_c=m_1$, which means that there is no lagging or advancing. In fact, for the case $\varepsilon_3=\varepsilon_1$, it indicates that there is no target in the background. Therefore, the method is valid for both dense targets and cavities. Denote compensated target points as $(\boldsymbol{R}^0,\boldsymbol{W}^0)$, where $\boldsymbol{R}^0=[x_{c1},\cdots,x_{cP}]^T$, $\boldsymbol{W}^0=[z_1,\cdots,z_P]^T$. Now the target points including both front and back surface can be expressed as

$$(\boldsymbol{R},\boldsymbol{W})=\left(\boldsymbol{R}^0,\boldsymbol{W}^0\right)\cup\left(\boldsymbol{R}^1,\boldsymbol{W}^1\right) \tag{7}$$

Step 6: All true target points of the shape are reconstructed, as shown in Fig. 2(g). Now consider the energy value assignment for each target points. Since the energy from the front surface is much stronger than that from the back surface, the average energy value of target points $(\boldsymbol{R}^1,\boldsymbol{W}^1)$ from the front surface is assigned to all target position values, i.e.,

$$T(\boldsymbol{R},\boldsymbol{W})=\frac{1}{W}\sum_{w=1}^{W}B\left(\boldsymbol{R}^1,\boldsymbol{W}^1\right) \tag{8}$$

Here T represents the energy value of points in $(\boldsymbol{R},\boldsymbol{W})$.

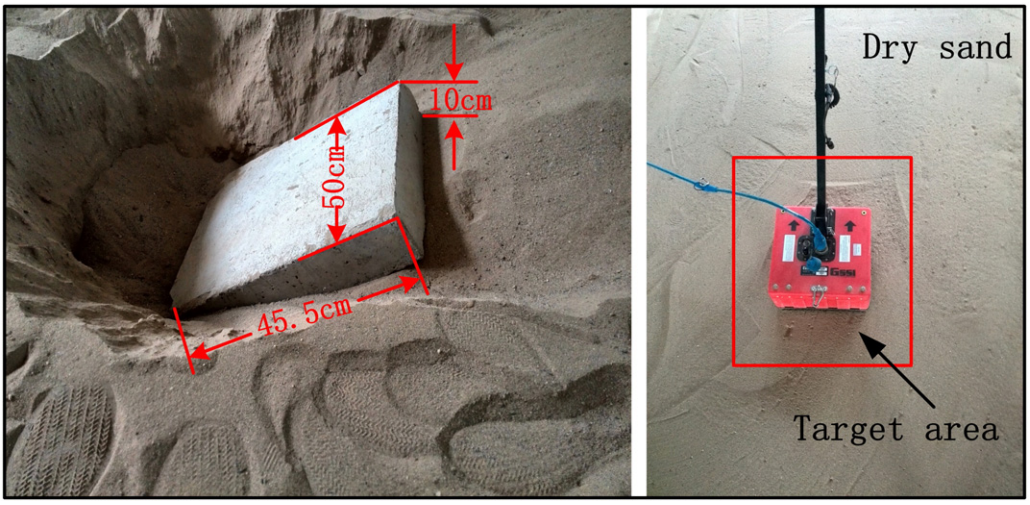

Fig. 3. Laboratory experiment scenario of subsurface sloped concrete slab.

In order to remove virtual image points, the virtual image energy value I can be replaced by the background value in Step 1.

$$I(x_{ki}, y_{ki}) = G(y_{ki}) \tag{9}$$

where $(x_{ki}, y_{ki}) \in (\boldsymbol{K}, \boldsymbol{S})$, $i = 1, 2, \ldots, S$. Then the geometric features such as the position, size, and shape of the target can be reconstructed, as shown in Fig. 2 (g).

4. Experiment results and analysis

The experiment is carried out in a sandbox and a concrete slab with its size 50 cm × 45.5 cm × 10 cm is buried obliquely in the sand, as shown in Fig. 3. Detailed parameters are given in Fig. 4. Here the sand layer is labeled as Layer 1 and the ground beneath the sand is indicated as Layer 2. The monostatic GPR is ground coupled radar from GSSI SIR-20 series. The antenna transmits Ricker wavelet with a center frequency of 400 MHz and pulse width of 2.5 ns. The scanning plane is divided into X and Y directions. There are 21 survey lines in Y direction with 5 cm interval. In each survey line the GPR moves along the test line in X direction with 1 cm interval. A B-scan contains 195 A-scans and each A-scan records 256 sampling points. Due to the limitation of space, the B-scan of the 11th survey line is analyzed to verify the performance of the proposed method. The results are derived via Matlab software.

Fig. 5(a) shows the B-scan energy image collected from the GPR system. The air–sand interface is labeled as interface 1 and the sand–ground interface is indicated as interface 2. It is difficult to determine target only from amplitude strength because of a large number of virtual image points shown in the box denoted with dot in Fig. 5(a). The high energy image in the box will be regarded as the target position without further analysis. In fact, the result hereinafter will show that virtual image may lead to the target position deviation. As analyzed in Step 2 and Step 3, phase information is displayed using Hilbert transform and then changes in phase are extracted by Eq. (3) (denoted by '*' in Fig. 5(b)).

When applying Step 4, virtual image points and true target points are discriminated, as denoted by 'O' and '*' in Fig. 6(a), respectively. As one expected, the high energy image in the dot box in Fig. 5(a) has been proved to be virtual image in Fig. 6(a). Note that in the

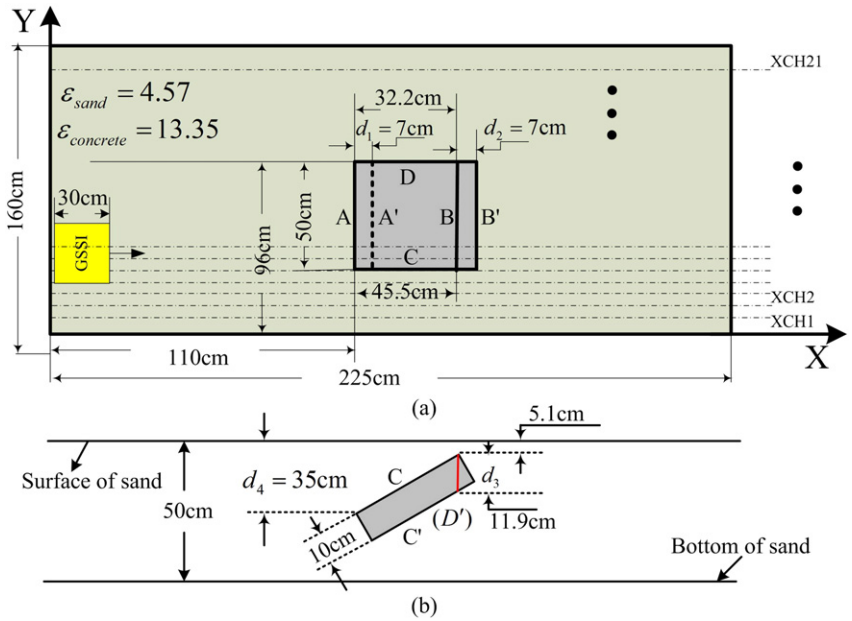

Fig. 4. Diagram for laboratory experiment parameters; (a) vertical view; (b) side view.

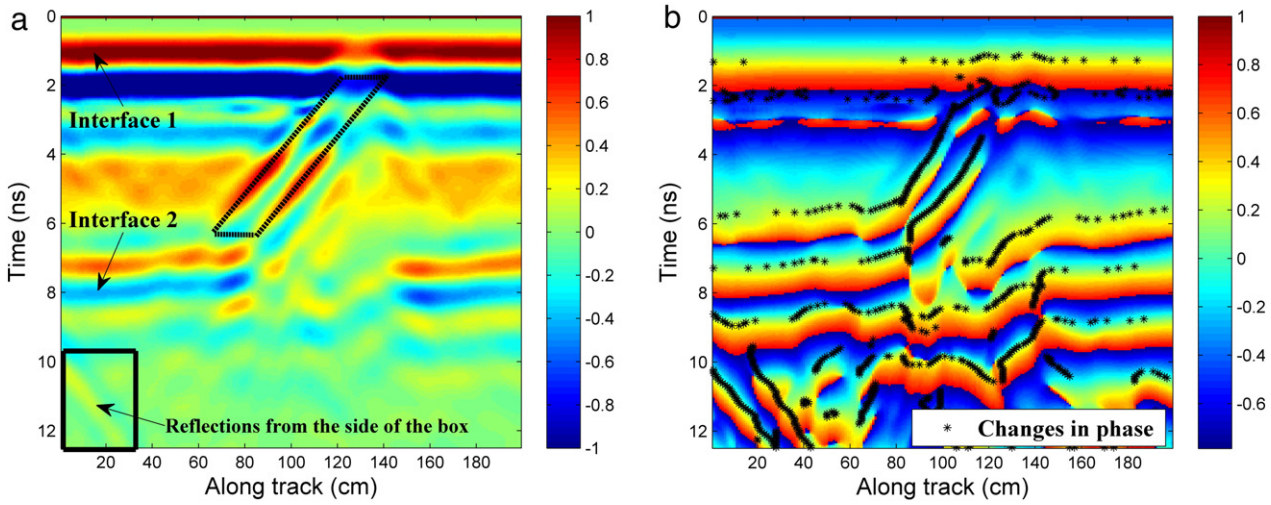

Fig. 5. (a) Scanning image based on amplitude; (b) phase information obtained by Hilbert transform and points of changes in phase.

experimental scenario, there exist clutters, which may be caused by surface roughness, inhomogeneous background, undesired reflectors, such as the sides of the sand-filled box. These will result in irrational points in both virtual image point set and true target point set. In order to remove those irrational points, we should exploit additional information. Firstly, the changes in phase from the lagging points indicate the horizontal boundary of the target, as shown with the red dashed line in Fig. 6(a). With this respect, the approximate boundary of the whole target can

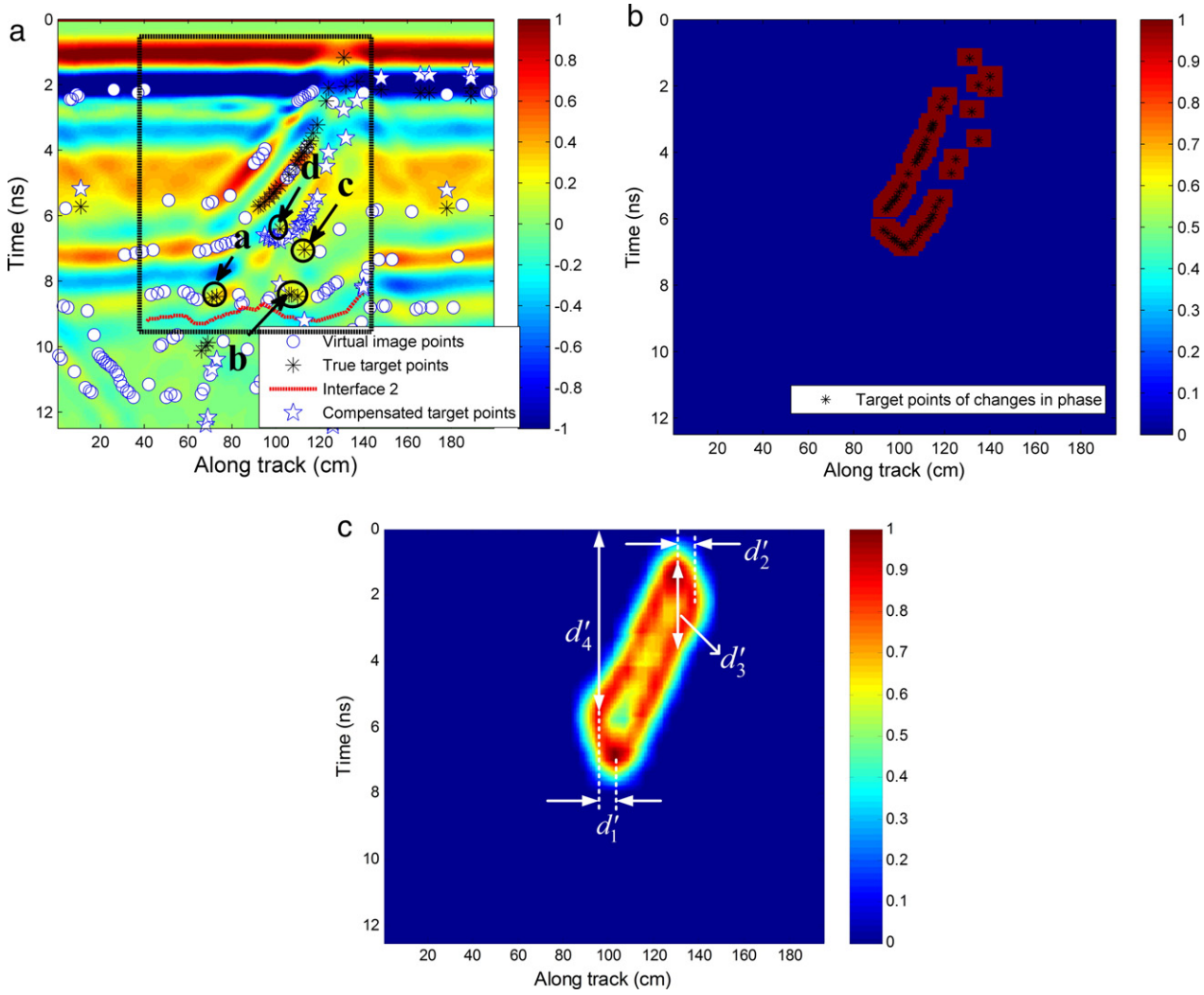

Fig. 6. (a) Virtual image and true target points are discriminated in Step 4; back surface points are compensated in Step 5; (b) target points of changes in phase and energy assignment for target points and background in Step 6; (c) reconstruction of the concrete slab profile of the 11th survey line after multidimensional filter.

Table 1
Reconstructed and experimental values.

Item	i			
	1	2	3	4
Reconstructed value d_i (cm)	7	7	11.9	35
Estimated value d_i' (cm)	8	8	9.24	38.79

be determined as shown with black dashed box in Fig. 6(a). In this case, the points outside the dashed box are regarded as irrational points and can be removed. Furthermore, in Step 5, the compensated back surface points shown as '★' in Fig. 6(a) should be also in the dashed box. Therefore, the compensated back surface points outside the box and their corresponding front surface points (as shown with circles a, b, and c in Fig. 6(a)) are removed. Then, the assumption in Step 5 that all true target points are regarded as front surface points indicates that all points of the back surface of the target are calculated, even if some back surface points of the target can be detected in Step 4, as shown with circle d in Fig. 6(a). In fact, the compensated back surface points calculated by its corresponding front surface point and the detected point d are quite close, even overlapped, according to Eq. (6). With this respect, the detected point d can be regarded as irrational points and removed to avoid duplication.

Until now the rational true target points have been chosen and thus the virtual image points and irrational target points are removed. Then the back surface points for the rational true target points are compensated by the procedure in Step 5. Combine those compensated points with rational true target points as the whole target points using Eq. (7), as shown in Fig. 6(b) with black '*'. Note that in the procedure of the energy value assignment for each target points, the pulse width Δp of EM wave should be considered. In practice, the target points are extended up to Δp/3 and assigned energy value by Eq. (8). Then, the remaining area is regarded as background and the energy value is replaced by Eq. (1) in Step 6, as shown in Fig. 6(b). Multidimensional filter is used to eliminate the effect of sharp boundary between target points and surrounding medium (Lu and Do, 2007). As detailed introduced by Lu and Do (2007), the directional filter bank is conducted for the image decomposed into subbands at different scales and directions. By this way, the image in Fig. 6(b) is filtered with an angle of 45° in a counterclockwise direction and the sharp boundaries are smoothed. The smoothed result of the reconstruction of the concrete slab profile of the 11th survey line is shown in Fig. 6(c).

Furthermore, some parameters from the reconstructed result and the experiment scenario are compared to verify the proposed method. The front edges A, B, C, and D of the concrete slab and their corresponding back edges A′, B′, C′, D′ are shown in Fig. 4. The horizontal distance between A and A′ labeled by d_1 is 7 cm. The horizontal distance between B and B′ labeled by d_2 is 7 cm. The vertical distance between front surface and back surface labeled by d_3 is 11.9 cm, as shown with red line in Fig. 4. The distance between the edge A and surface of the sand labeled by d_4 is 35 cm. These four parameters are labeled by d_1', d_2', d_3', and d_4' in Fig. 6(c), respectively. The reconstructed values and the experimental values are displayed in Table 1. It can be observed that the concrete slab under the ground in the example is left undistorted after applying the proposed method.

Apply the proposed method to other B-scan profiles from survey lines in Y direction. Then all the reconstructions from 21 survey lines are combined to form a 3-D image. The observation angle of azimuth −3.5° and elevation 15° is given in Fig. 7(a). As it clearly appears, the front surface and back surface of the concrete are displayed in along track range 93 cm to 140 cm. The observation angle of azimuth −67.5° and elevation 10° is given in Fig. 7(b). The concrete slab appears in cross track range 45 cm to 89 cm. It can be observed that there exists a little energy in cross track range 30 cm to 43 cm. This is caused by the fact that the GPR records signals at the non-target area due to the radar lobes. It is also worth to be noted that there exist clutters in the laboratory experiment. Nevertheless, those results show a good reconstruction of the size and shape of the subsurface concrete slab and prove the validity and robustness of the proposed method.

5. Conclusion

In this paper, we have developed a novel method for reconstruction of subsurface large sloped dielectric target. Compared to the traditional reconstruction method based on the amplitude for small target, problems for such large sloped dielectric target were proposed, i.e., virtual image interference and weak energy detection. Considering the good advantage of phase, changes in phase were developed to highlight the characteristic of a target. In order to eliminate virtual image, we employed the method based on the geometric relationship between the recorded signal beneath the receiving antenna and the reflected signal emanated from the target position which is "ahead" or "behind" of the receiving antenna. With this method, most of the true target points from the front surface of the target were distinguished from the virtual image points. Subsequently, those extracted true target points were utilized to compensate the scattering centers of back surface of the target, under the contribution from the lagging or advancing points. By comparing some specific distance parameters of the reconstructed target with those set in the real site experiment, the results showed a

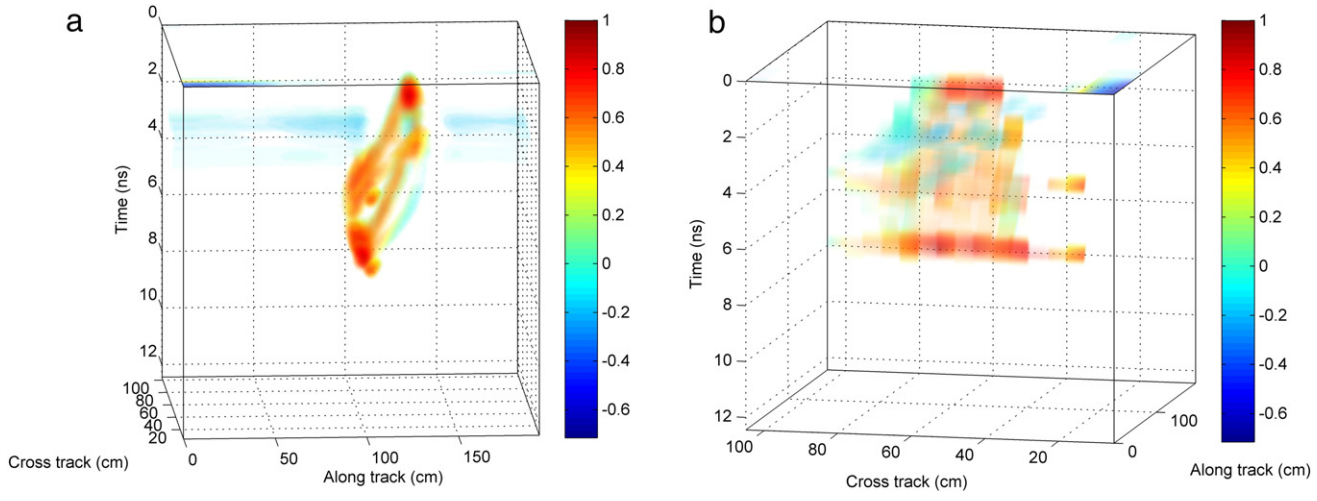

Fig. 7. 3-D reconstruction of subsurface concrete at observation angle of (a) (−3.5°,15°); (b) (−67.5°,10°).

good agreement. Finally, a 3-D image of the target was given to verify the effectiveness and robustness of the proposed method. Further work will be done to apply the method to the data collected from a field survey and multiple large targets with different inclined angles buried inside the sand layer will be considered.

Acknowledgment

The authors acknowledge support from the National Natural Science Foundation of China (No. 61371186) and Natural Science Foundation of Guangxi Province, China (No. 2013GXNSFFA019004).

References

Catapano, I., Crocco, L., Isernia, T., 2007. On simple methods for shape reconstruction of unknown scatterers. IEEE Trans. Antennas Propag. 55 (5), 1431–1436.
Catapano, I., Crocco, L., Isernia, T., 2008. Improved sampling methods for shape reconstruction of 3-D buried targets. IEEE Trans. Geosci. Remote Sens. 46 (10), 3265–3273.
Chlaib, H., Mahdi, H., et al., 2014. Using ground penetrating radar in levee assessment to detect small scale animal burrows. J. Appl. Phys. 103, 121–131.
Daniels, D.J., 2004. Ground Penetrating Radar. 2nd ed. The Institution of Electrical Engineers, London, UK.
Hipple von, A., 1995. Dielectrics and Waves. 1st ed. Artech House, USA.
Huuskonen, E., Mikhnev, V., Olkkonen, M., 2015. Discrimination of buried objects in impulse GPR using phase retrieval technique. IEEE Trans. Geosci. Remote Sens. 53 (2), 1001–1007.
Liu, S., Wei, Y., 2015. Fast nearest neighbor searching based on improved VP-tree. Pattern Recogn. Lett. 60–61, 8–15.
Lu, Y.M., Do, M.N., 2007. Multidimensional directional filter banks and surfacelets. IEEE Trans. Image Process. 16 (4), 918–931.
Mikhnev, V., Olkkonen, M., Huuskonen, E., 2012. Identification of buried objects in GPR using phase information extracted from transient response. Proceedings of the 9th European Radar Conference, Amsterdam, The Netherlands, pp. 322–325.
Neto, P., Medeiros, W., 2006. A practical approach to correct attenuation effects in GPR data. J. Appl. Phys. 59 (2), 140–151.
Ni, X., Huo, X., 2007. Statistical interpretation of the importance of phase information in signal and image reconstruction. Stat. Probab. Lett. 77, 447–454.
Nomura, Y., Kato, N., Naganuma, Y., et al., 2011. A geometrical analysis of buried flat-plates on ground penetrating radar images. ICSMC 2011, 3317–3322.
Schofield, J., Daniels, D., et al., 2014. A multiple migration and stacking algorithm designed for land mine detection. IEEE Trans. Geosci. Remote Sens. 52 (11), 6983–6988.
Skolnik, M., 2008. Radar Handbook. 3rd ed. The McGraw-Hill Companies, USA.
Soldovieri, F., Brancaccio, A., Leone, G., Pierri, R., 2005. Shape reconstruction of perfectly conducting objects by multiview experimental data. IEEE Trans. Geosci. Remote Sens. 43 (1), 65–71.
Sugak, V., Sugak, A., 2010. Phase spectrum of signals in ground-penetrating radar applications. IEEE Trans. Geosci. Remote Sens. 48 (4), 1760–1767.
Taner, T., 2001. Seismic attributes. CSEG Recorder, September, pp. 49–56.
Valerio, G., Soldovieri, F., Barone, P.M., et al., 2011. Shape reconstruction of scatterers by suitable inverse processing of GPR data. 6th (EUCAP), pp. 2209–2211.
Walton, G., Lato, M., Anschutz, H., et al., 2015. Non-invasive detection of fractures, fracture zones, and rock damage in a hard rock excavation-experience from the Aspo Hard Rock laboratory in Sweden. Eng. Geol. 196, 210–221.